Vietnam Journal of Catalysis and Adsorption
Tạp chí xúc tác và hấp phụ Việt Nam

http://chemeng.hust.edu.vn/jca/

# Sol-gel synthesis and characterization of neodymium orthoferrite for disposing oily wastewater

Thi To Nga Phan*, Thi Hai Nam Chu

*School of Chemical Engineering, Hanoi University of Science and Technology*
**Email: nga.phanthito@hust.edu.vn*

ARTICLE INFO

Received: 30/3/2023
Accepted: 06/6/2023
Published: 30/6/2023

*Keywords:*
$NdFeO_3$, sol-gel, photo-Fenton, visible light, oily wastewater

ABSTRACT

The aim of this study was to design and characterize a $NdFeO_3$-based photocatalyst prepared by sol-gel method for treatment of oily wastewater. Different characterization techniques such as X-ray diffraction (XRD), scanning electron microscope (SEM), Fourier transform infrared spectroscopy (FTIR), UV–vis spectrophotometer were used to elucidate the structure, morphology, surface functional groups, and optical absorption properties of the prepared $NdFeO_3$ photocatalyst. The photo-Fenton degradation performance of the as-prepared $NdFeO_3$ photocatalyst was investigated by degrading oily-containing wastewater under visible light irradiation. The $NdFeO_3$ photocatalyst manifests the high chemical oxygen demand (COD) removal efficiency of 97.6 % for 120 min reaction) thanks to its narrow band gap energy and high crystalline degree.

## Introduction

Photo-Fenton catalysis process is one of the most emerging processes for environmental remediation because it is a clean technique and effectively usage of ultraviolet or visible light. These processes produce OH radicals (•OH), which are extremely reactive with oxidation potential of 2.8 V and attack most organic molecules [1]. However, the main issue with photocatalysis is its high cost. The utilization of solar energy for this process could help to overcome that problem by decreasing the energy consumption required to generate UV radiation. From the practical application point of view, heterogeneous photo-Fenton process employing the solar technologies has been most extensively studied and developed.

Heterogeneous photo-Fenton catalysis *via* semiconducting oxides such as $TiO_2$, ZnO or $Fe_2O_3$ is considered as the common photo-Fenton catalysts for degradation of organic pollutants in wastewater [2-4]. However, the photo-Fenton catalytic efficiencies of these materials are still limited. In order to overcome these problems, perovskite-type semiconductors have attracted considerable attention for use as photocatalysts to remove toxic organic compounds. Perovskite-type oxides have general formula of $ABO_3$, where A is the rare earth and B is the transition metals, respectively. Neodymium orthoferrite ($NdFeO_3$) perovskite is an important p-type semiconductor with excellent physical and chemical properties. It has widely been used in many applications such as sensor [5], photocathodes [6], fuel cells [7], and catalysts [8, 9]. Noting that, the properties of $NdFeO_3$ are strongly dependent on the preparation method, which has a great influence on their crystalline structure, morphology, particle size, and especially photocatalytic performance. Several synthetic methods were

https://doi.org/10.51316/jca.2023.027

employed to synthesize $NdFeO_3$, such as co-precipitation method [10], sol–gel method [11], hydrothermal route [12], ultrasound process [13], and solid-state method [14].

Recently, several research groups have employed the sol-gel method for the preparation of semiconducting materials. Sol-Gel method is one of the simplest techniques to synthesize high-quality nano and microstructures. This method offers several advantages over other synthesis routes such as control over the texture, size and surface properties of the materials, easy to implement, low cost, high quality, and production of materials with large surface areas [15]. This flexibility and simplicity make it very popular in the production of nanoscale powders. One of the most significant advantages of this process is its simplicity and the low-temperature precursor handling. This causes the formation of nanopowders with excellent purity and uniformity, and precise control of the final composition of the material. For example, Shlapa et al. [16] prepared a homogenous $La_{1-x}Sr_xMnO_3$ ($0.23 < x < 0.25$) nanoparticles with a very narrow particle sizes ranging in 30–35 nm. They reported that the precursor arises during the reaction between metal ions and organic compounds (citric acid and ethylene glycol) and pyrolysis of the resulting gel. In another work, Liu et al. [17] synthesized $LaMnO_3$ with high surface area using citric acid and EDTA as chelating agents. The results showed that EDTA-citrate generated smaller nanoparticles than the single citrate acid. The samples exhibited a high specific surface area showing excellent oxygen reduction and evolution reaction catalytic performance.

The aim of the research is to fabricate $NdFeO_3$ nanoparticles using a facile sol-gel method following by high temperature calcination. The effect of the synthetic method on the crystallinity, morphology, and band gap energy of obtained sample was investigated. In this research, the photocatalytic activities of the as-synthesized $NdFeO_3$ nanoparticles were also examined in detail by photo-Fenton degradation of oily wastewater under visible light irradiation.

## Materials and methods

### *Materials*

Neodymium nitrate hexahydrate ($Nd(NO_3)_3{\cdot}6H_2O$; 99.9%), Iron nitrate nonahydrate ($Fe(NO_3)_3{\cdot}9H_2O$; 98–101), citric acid ($C_6H_8O_7{\cdot}H_2O$; ≥99.5%), hydrogen peroxide solution ($H_2O_2$, 30%), and ethanol ($C_2H_5OH$, 95%) were purchased from Sigma-Aldrich. All chemicals were used without additional purification.

### *Synthesis of $NdFeO_3$ by solgel method*

$NdFeO_3$ was synthesized *via* sol-gel method [8]. Typically, 10 mmol $Nd(NO_3)_3.6H_2O$, 10 mmol $Fe(NO_3)_3.9H_2O$ and 20 mmol citric acid was dissolved in a mixture of 10 mL DI water and 20 mL of ethanol to form a homogeneous solution at room temperature. After that, the resulting suspension was stirred at room temperature for 3 h and then at 70 °C to evaporate the solvent, followed by drying at 80 °C overnight and then calcination at 800 °C (heating rate of 2 °C/min from room temperature to 800 °C). Finally, the obtained powder $NdFeO_3$ was denoted as NFO.

### *Characterizations of $NdFeO_3$*

Powder X-ray diffraction (XRD) patterns of sample was analyzed on a Bruker D8 diffractometer (Bruker, USA) using CuKα as radiation. The data was collected in 2θ range from 10 to 80° with a step size of 0.02°/s. Scanning electron microscopy (SEM) (Zeiss 1555 VP-FESEM, Germany) was employed to determine the surface morphology of the sample. Transmission Electron Microscopy (TEM) analysis was performed on TEM-TITAN operating at 200 kV. Fourier transform infrared (FTIR) spectra were recorded on a FTIR spectrometer (JASCO FT/IR-4600) using the KBr pellet technique. The optical absorption spectra were recorded from 200 to 800 nm on a PerkinElmer LAMBDA 750 UV/Vis/NIR spectrophotometer (PerkinElmer, USA). The band gap value was calculated from the interception of a linear fitted to the low energy side in a plot of $[F(R)h\nu]^2$ versus $h\nu$ ($h\nu$: the energy of the incident photon; F(R): the Kubelka Munk function); F(R) was calculated as below equation [18]:

$$F(R) = \frac{(1-R)^2}{2R}$$

in which R is reflectance.

### *Photo-Fenton degradation of oily wastewater*

Photocatalytic activity of NFO was examined by adding 1 g/L NFO into 100 mL of oily wastewater in a cylindrical vessel, which was surrounded by a circulating water jacket to maintain solution temperature at ambient temperature. A photo-Fenton-like reaction was initiated by introducing 1 mL $H_2O_2$ to the suspension. A Xenon lamp (CEL-HX F300) with a 400 nm cut-off filter was used as a visible light source

for photocatalytic degradation test. Prior to light irradiation, the suspension was magnetically stirred in dark for 30 min to reach an adsorption-desorption equilibrium of solution. Subsequently, the suspension was exposed to visible light for 90 min and 3 mL of the sample was taken from the suspension every 15 min and was filtered by filter papers (0.22 µm Millipore Durapore membrane, 40 Ashless, diameter 150 mm) to separate the solid catalyst. The obtained supernatant was tested by the quantification of chemical oxygen demand (COD). COD was measured by COD photometer (manufactured by CHEMetrics). The COD removal rate (%) was calculated using formula given below:

$$COD\ removal\ rate\ (\%) = \left(1 - \frac{COD_t}{COD_0}\right) \times 100\%$$

where $COD_0$ and $COD_t$ are the COD values of oily wastewater before and after time *t* in the photo-Fenton degradation.

## Results and discussion

### *XRD analysis*

XRD analysis of NFO sample is shown in Fig. 1. Fig. 1 reveals the crystalline nature of NFO. All diffraction peaks could be indexed to the orthorhombic perovskite $NdFeO_3$ (JCPDS No. 37-1493) [19]. No other impurity phases have been observed, implying that the as-prepared sample is single phase NFO. Using the Scherrer formula [20], the average particle size of the NFO sample was found to be 19.4 nm based on the (121) peak.

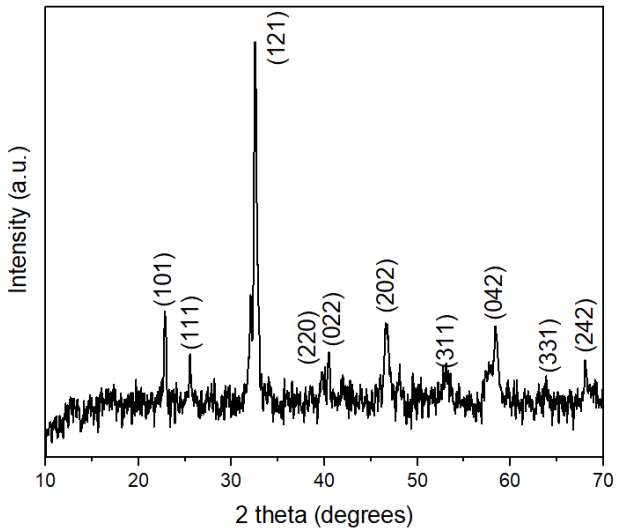


Figure 1: XRD pattern of $NdFeO_3$

### *Fourier Transform Infrared Spectroscopy (FTIR)*

Figure 2 shows FTIR spectra of as-prepared NFO sample in the range from 4000 - 400 $cm^{-1}$. As can be seen clearly from Fig. 2 that the asymmetric stretching of carbonates has been reported at 1505 and 1342 $cm^{-1}$, respectively [21], suggesting that carbonate species (as a result of exposure to the ambient air) form on the NFO surface. However, the presence of the species cannot be detected by XRD analysis. Based on the literature survey, the sharp absorption band at 546 $cm^{-1}$ could be attributed to Fe-O stretching vibration, being characteristics of the octahedral $FeO_6$ group in NFO, which was commonly observed in the region 500-700 $cm^{-1}$ [22]. This observation agrees with the result obtained from XRD analysis that the single crystalline NFO phase has already been formed at 800 °C.

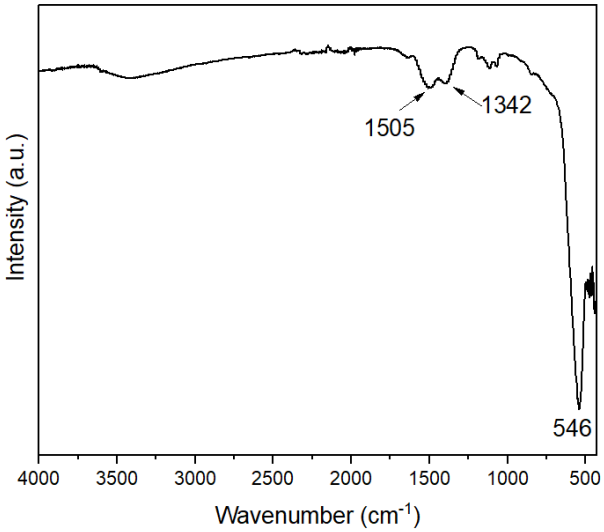


Figure 2: FTIR spectra of $NdFeO_3$

### *Scanning Electron Microscope (SEM)*

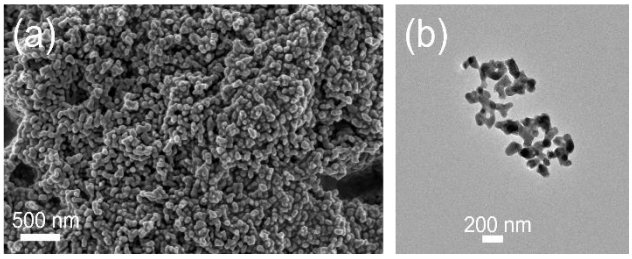


Figure 3: (a) SEM image and (b) TEM image of $NdFeO_3$

The morphology of the NFO sample was studied by SEM, as illustrated in Figura 3a. It is observed that the particles of NFO showed agglomerated spherical morphology with a diameter of approximately 50 nm – 100 nm. The merit of sol-gel method for synthesizing the NFO sample has been proven by fabricating NFO with small particle size. Further insight into the

morphology of NFO nanoparticles was provided by TEM image in Figure 3b. The NFO showed uniform $NdFeO_3$ nanosphere morphology with diameters between 50 and 100 nm, which is consistent with SEM observation.

### *Optical property*

It is well known that optical properties have an influence on the photocatalytic performances of photocatalysts. Thus, tailoring of a photocatalyst having an optimum band gap, which can harvest the visible light has become the emerging objective recently. The UV-Vis absorption spectra and the corresponding band gap energy of NFO are shown in Figure 4. Interestingly, the NFO sample has suitable band gap energy for organic pollutant degradation under visible light irradiation. It can be seen from Fig. 4 that the absorption spectra of NFO showed strong absorption in the visible region (400–800 nm). The optical band gap of the material can be determined from the reflectance spectral data according to the Kubelka-Munk equation. The band gap value of the NFO was found to be 2.29 eV as shown in the inset of Figure 4. Obviously, the narrow band gap energy of NFO would be the favorable characteristic for harvesting more photons from visible light source and in turn enhancing the photocatalytic activity of catalysts.

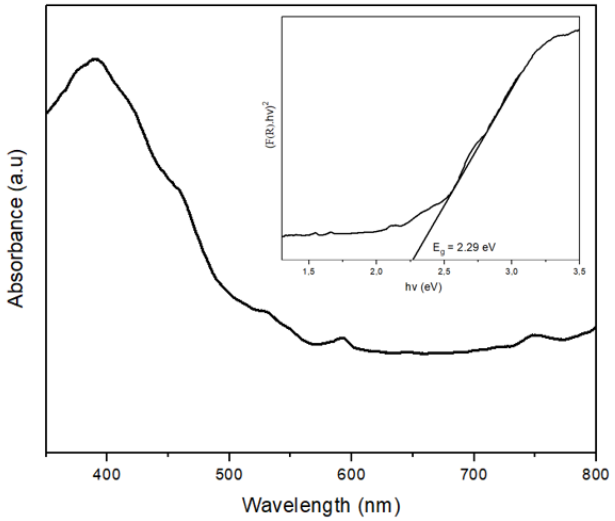


Figure 4: UV-Vis absorption spectra of $NdFeO_3$ (the inset is the plot of $(F(R)h\nu)^2$ versus hν)

### *Photo-Fenton degradation of oily wastewater*

In the photo-Fenton catalyst of NFO process under visible light irradiation, the photocatalyst NFO is one of the key factors that determine the operational efficacy of photo-Fenton degradation of oily wastewater. Particularly, Figure 5 illustrated the COD removal rate of the photodegradation of oily wastewater in various reaction conditions under visible light irradiation such as in the presence only oily wastewater or $H_2O_2$ or NFO, and in the simultaneous presence of NFO and $H_2O_2$. It should be noted that no degradation of oily wastewater was observed under dark conditions (which is not shown here). As can be seen clearly from the Figure 5 that oily wastewater was hardly degraded under visible light illumination only while the COD removal rate was found to be 9.6 % in the presence of 10 mM $H_2O_2$.

The COD removal rate was slightly improved (53.9 %) when using 1 g/L NFO as a photocatalyst within 120 min. Meanwhile, significant degradation was observed under visible light irradiation when both NFO and $H_2O_2$ (with the similar concentration as other mentioned systems) were present, which suggests NFO as a heterogeneous visible-light-driven Fenton-like catalyst. The COD removal *via* photo-Fenton degradation in the system using NFO was the highest compared to that of other systems, being 97.6 %.

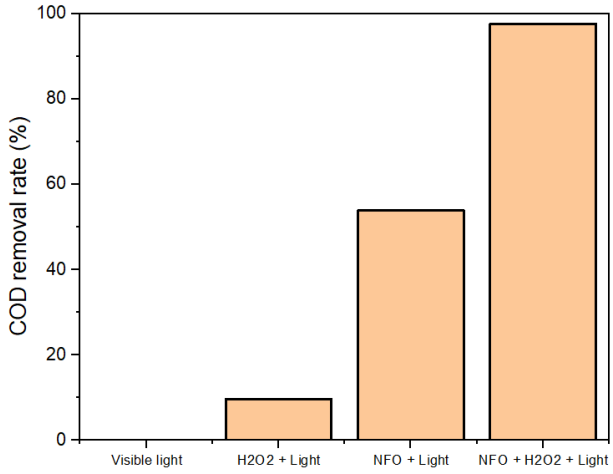


Figure 5: COD removal efficiencies by the photo-Fenton degradation of oily wastewater over NFO photocatalyst

In photo-Fenton process over NFO photocatalyst, the reaction is activated by absorption of a photon with sufficient energy (equal or higher than the band-gap energy of the NFO photocatalyst). The absorption leads to a charge separation due to promotion of an electron ($e^-$) from the valence band of the NFO catalyst to its conduction band, thus generating a hole ($h^+$) in the valence band [23]. The relevant reactions at the NFO surface governing the degradation of pollutants

in oily wastewater can be expressed as the following equations:

$NFO + hv \rightarrow NFO\ (e^- + h^+)$ (1)

$H_2O_2 + e^- \rightarrow {}^{\bullet}OH + OH^-$ (2)

In the other words, NFO acts as a heterogeneous photo-Fenton catalyst, which participates in a typical Fenton-like reaction, the commonly accepted mechanism is as follows [24]:

$Fe^{3+} + H_2O_2 \rightarrow Fe^{3+}\ H_2O_2$ (4)

$Fe^{3+}\ H_2O_2 \rightarrow Fe^{2+} + HO_2{}^{\bullet} + H^+$ (5)

$Fe^{3+} + HO_2{}^{\bullet} + H^+ \rightarrow Fe^{2+} + O_2 + 2H^+$ (6)

$Fe^{2+} + H_2O_2 \rightarrow Fe^{3+} + {}^{\bullet}OH + OH^-$ (7)

Obviously, the presence of NFO and $H_2O_2$ is essential for the generation of hydroxyl radicals (•OH) which directly oxidizes pollutants presenting in oily wastewater under visible light irradiation to form degradation products, as Eq.8 [25]:

${}^{\bullet}OH$ + hydrocarbons → Degradation products (8)

## Conclusions

The photo-Fenton catalyst NFO synthesizing by sol-gel method possesses high photo-Fenton catalytic degradation of oily wastewater under visible light thanks to its high crystallinity, small particle size, and narrow band gap energy. The maximum COD removal efficiency of 97.6 % was observed when adding 1 g/L NFO and 10 mM $H_2O_2$ simultaneously into 100ml oily wastewater, and carried out photo-Fenton process under visible light irradiation within 120 min. The synthetic method of photocatalyst is simple, fast, and cost effective which could be the potential approach for the synthesis of future perovskite-based photocatalysts.

## Acknowledgement

This research is funded by Vietnam Ministry of Education and Training under grant number B2021-BKA-15.

## References

1. De-Nasri, S.J., et al., Chem. Engi. J. 420 (2021) 127560. https://doi.org/10.1016/j.cej.2020.127560
2. Hernández-Coronado, E.E., et al., J. Environ. Chem. Eng. 9(6) (2021) 106822. https://doi.org/10.1016/j.jece.2021.106822
3. Hassaan, M., et al., Egyptian J. Chem. 63(4) (2020) 1443-1459. http://doi.org/10.21608/EJCHEM.2019.15799.1955
4. Li, J., et al., J. Environ. Chem. Eng. (2022) 108329. https://doi.org/10.1016/j.jece.2022.108329
5. Rajaitha, P.M., et al., J. Alloys Compd. 915 (2022) 165402. https://doi.org/10.1016/j.jallcom.2022.165402
6. Quiñonero, J., et al., ACS Appl. Mater. Inter. 13(12) (2021) 14150-14159. https://doi.org/10.1021/acsami.0c21792
7. Tongyun, C., et al., J. Rare Earths 30(11) (2012) 1138-1141. https://doi.org/10.1016/S1002-0721(12)60194-X
8. Prabagar, J.S., et al., Mater. Today: Proceedings 75 (2023) 15-23. https://doi.org/10.1016/j.matpr.2022.10.230
9. Omari, E. and M. Omari, Inter. J. Hydro. Ener. 47(32) (2022) 14542-14551. https://doi.org/10.1016/j.ijhydene.2022.02.197
10. Khorasani-Motlagh, M., et al., Inter. J. Nanosci. Nanotechnol. 9(1) (2013) 7-14.
11. Shanker, J., et al., Phys. Letters A 382(40) (2018) 2974-2977. https://doi.org/10.1016/j.physleta.2018.07.002
12. Wang, Y., et al., CrystEngComm 16(5) (2014) 858-862. https://doi.org/10.1039/C3CE41434E
13. Yousefi, M., S. Zeid, and M. Khorasani-Motlagh, Current Chem. Let. 6(1) (2017) 23-30. http://doi.org/10.5267/j.ccl.2016.10.002
14. Pokhriyal, P., et al., ECS J. Solid State Sci. Technol. 10(7) (2021) 073005.
15. Danks, A.E., S.R. Hall, and Z. Schnepp, Mater. Horizons 3(2) (2016) 91-112. http://doi.org/10.1149/2162-8777/ac10cc
16. Shlapa, Y., S. Solopan, and A. Belous, J. Mag. Mag. Mater. 510 (2020) 166902. https://doi.org/10.1016/j.jmmm.2020.166902
17. Li, C., et al., J. Phys. Chem. Solids 113 (2018) 151-156. https://doi.org/10.1016/j.jpcs.2017.10.039
18. Albadi, Y., et al., Inorganics 9(5) (2021) 39. https://doi.org/10.3390/inorganics9050039
19. Wang, Y., et al., Mater. Let. 60(13-14) (2006) 1767-1770. https://doi.org/10.1016/j.matlet.2005.12.015

20. Xu, L., et al., World J. Nanosci. Eng. 2 (2012) 154-160. http://doi.org/10.4236/wjnse.2012.23020
21. Li, X., et al., Chem. Mater. 22(17) (2010) 4879-4889. https://doi.org/10.1021/cm101419w
22. Singh, S., et al., Sensors Actuat. B: Chem. 177 (2013) 730-739. https://doi.org/10.1016/j.snb.2012.11.096
23. Ren, G., et al., Nanomater. 11(7) (2021) 1804. https://doi.org/10.3390/nano11071804
24. Phan, T.T.N., T.T.N. Phan, and T.H. Pham, J. Porous Mater. (2022) 1-12. https://doi.org/10.1007/s10934-022-01378-z
25. Phan, T.T.N., et al., Appl. Surf. Sci. 491 (2019) 488-496. https://doi.org/10.1016/j.apsusc.2019.06.133